SCIENCE CHINA
Information Sciences

• RESEARCH PAPER •
Special Focus on Space Flexible Manipulation and Control for On-orbit Servicing

May 2017, Vol. 60 050204:1–050204:14
doi: 10.1007/s11432-016-9034-7

Analysis and design of parameters in soft docking of micro/small satellites

Xiang ZHANG*, Yiyong HUANG & Xiaoqian CHEN

College of Aerospace Science and Engineering, National University of Defense Technology, Changsha 410073*, China*

Received December 18, 2016; accepted January 17, 2017; published online April 1, 2017

Abstract Although substantial research has been conducted on the soft docking problem, the design of the docking mechanism is always conducted using experience. The challenge for conducting factor analysis and design lies in an accurate theoretical model, and the evaluation criteria of a successful docking. In this paper, the soft docking model of micro/small satellites is proposed using an analytical method and validated using a commercial FE package. The evaluation criterion of a successful docking is defined by considering the operational principle of the capturing mechanism used in micro (or small) paired satellites. The effect of the parameters on the soft docking result is discussed and their value domains are designed based on our proposed criteria of a successful docking.

Keywords soft docking, micro/small satellite, flexible beam, analytical method, analysis, design

Citation Zhang X, Huang Y Y, Chen X Q. Analysis and design of parameters in soft docking of micro/small satellites. Sci China Inf Sci, 2017, 60(5): 050204, doi: 10.1007/s11432-016-9034-7

1 Introduction

With the booming development of micro and small satellites, many colleges and corporations have sent their small satellites into space. Meanwhile, the docking mechanisms for micro and small satellites give a hot topic that attracts many researchers [1–3]. The concept of a soft docking between two space vehicles is primarily seen in the patent of a magnetic docking probe [4]. It is helpful to conduct the capture and connection between two satellites by adopting the scheme of soft docking. Among these docking mechanisms, a new docking concept using a flexible beam to replace the docking probe is proposed [5]. The space probe cone docking system is a rigid-flexible coupling dynamic system. The vibration of the flexible beam stimulated by the impact between docking probe and docking cone will influence the motion of the dynamical system.

To solve the rigid flexible dynamic problem during the docking process, the Lagrange analytical method provides an easy way with general expressions. Yoo et al. [6, 7] investigated a rotating cantilever beams with a concentrated mass located at an arbitrary position. Hong et al. [8, 9] studied the impact dynamics of a planar flexible multi-body system. However, the modeling process of the Lagrange method includes many integral differential operations. To reduce such complexity, the Kane method was developed by

* Corresponding author (email: zxstudy@hotmail.com)

combining the advantages of vector mechanics and analytical mechanics. The Kane equation was firstly published in 1987 by Kane [10]. Pellicano et al. [11] analyzed the dynamic behavior of a simply supported beam subjected to an axial transport of mass. Yoo et al. [12, 13] derived the equations of beam motion using the Kane method. Cai et al. [14] investigated the frequency characteristics of a flexible hub beam system with an attached mass. To solve the vibration of a flexible beam stimulated by the docking impact, the assumed mode method (AMM) is coupled into the Lagrange or the Kane equations. The AMM is a classical method used to describe the dynamical performance of a flexible beam [15, 16]. Ni et al. [17] presented a method to investigate the natural frequencies of the beam system using AMM. Xi et al. [18] investigated the free transverse vibration of a standing and hanging Rayleigh beam-column subjected to vertically orientated gravity load using AMM. Moreover, an investigation on the modeling of the docking process has been conducted by some researchers [19–22]. Although substantial research has been conducted on the docking problem, the design of the docking mechanism is always conducted using experience. The challenge for conducting factor analysis and design lies in an accurate theoretical model and the evaluation criterion of a successful docking.

The purpose of this paper is to design the parameters of the soft docking of micro/small satellites. The paper is organized as follows. In Section 2, the soft docking model of micro/small satellites is proposed using the Kane method and the validation using a commercial FE package is presented. The evaluation criteria for a successful docking are defined by considering the operational principle of the capturing mechanism used in micro (or small) paired satellites. In Section 3, the effect of the main factors on the soft docking result is discussed. Their value domains are designed based on our proposed successful docking criteria. Finally, conclusion is presented in Section 4.

2 Prediction and evaluation of soft docking

2.1 Soft docking model of micro/small satellites

To simplify the modeling of the soft docking of micro/small satellites, it is assumed that the motion of the central axes of the satellites stays in one plane during the whole docking process. Thus, the docking problem can be studied in a single plane as shown in Figure 1.

In Figure 1, $o-\boldsymbol{ij}$ is the inertial coordinate frame. $o_1-\boldsymbol{i}_1\boldsymbol{j}_1$ and $o_2-\boldsymbol{i}_2\boldsymbol{j}_2$ are the body-fixed coordinate frames. o_1 and o_2 are the mass centers of the chaser satellite and the target satellite respectively. The docking probe is mounted on the chaser satellite, and the docking cone is mounted on the target satellite. In Figure 1(a), a is the distance from the mass center of the chaser satellite to the end of the docking probe. l_1 and d_1 are the length and diameter of the docking probe respectively. l_2 is the cone length. R_2 is the radius of the inner cone. β is half of the cone angle. c is the distance from the mass center of the target satellite to the inner cone edge. In Figure 1(b) and (c), m_1 and I_1 are the mass and mass inertia moment of the chaser satellite respectively, while m_2 and I_2 are the mass and mass inertia moment of the target satellite respectively. θ_1 and θ_2 are the rotational angles of the chaser satellite and the target satellite respectively, while $\boldsymbol{\omega}_1$ and $\boldsymbol{\omega}_2$ are their angular velocities. v is the lateral deflection stimulated by the contact between the docking probe and the docking cone. u is the axial displacement related with the lateral deflection. b is a distance used to record the contact point. F_N and F_τ denote the normal and the tangential contact forces, respectively, which can be obtained using the Hertz contact theory [5]. The soft docking of micro/small satellites is modeled by analytical method. The model is developed in two sections, which are the equations of the chaser satellite and the equations of the target satellite. Details are provided in the following sections.

2.1.1 *Equations of the chaser satellite*

In Figure 1, it is seen that the chaser satellite is a rigid flexible coupling system that includes the satellite body and the flexible docking probe. The satellite body is simplified as a rigid cubic mass and the docking probe is studied using a flexible beam model. The AMM is adopted to describe the dynamical

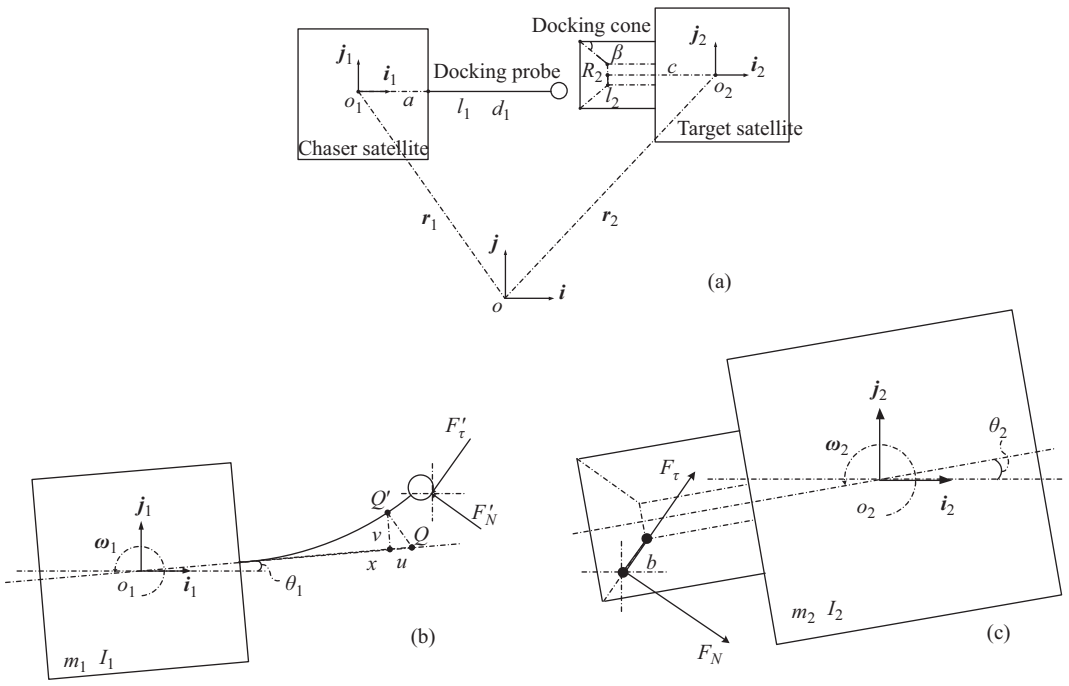

Figure 1 Soft docking of micro/small satellites. (a) Prior to docking; (b) chaser satellite during docking; (c) target satellite during docking.

performance of the flexible beam. The lateral deflection is given by

$$v(x,t)=\sum_{i=1}^{n}\varphi_i(x)q_i(t). \tag{1}$$

The axial displacement related with the lateral deflection is obtained by

$$u(x,t)=-\frac{1}{2}\int_0^x\left(\frac{\partial v(\sigma,t)}{\partial\sigma}\right)^2\mathrm{d}\sigma. \tag{2}$$

Accordingly, the independent speed variables of the chaser satellite are defined as $\dot{u}_1$, $\dot{v}_1$, $\dot{\theta}_1$, $\dot{q}_1$, $\dot{q}_2$, $\ldots,\dot{q}_n$. Based on these independent speed variables (n+3), the Kane equations of the chaser satellite are composed of the contributions of the flexible beam and the rigid satellite body.

First, the contributions of the flexible beam are deduced. In Figure 1(b), the displacement vector of point Q' in the inertia frame is given by

$$\begin{aligned}\boldsymbol{r}(x,t)=&\{u_1+[a+x+u(x,t)]\cos(\theta_1)-v(x,t)\sin(\theta_1)\}\boldsymbol{i}\\&+\{v_1+[a+x+u(x,t)]\sin(\theta_1)+v(x,t)\cos(\theta_1)\}\boldsymbol{j}.\end{aligned} \tag{3}$$

The corresponding velocity vector is given by

$$\begin{aligned}\boldsymbol{V}(x,t)&=\dot{\boldsymbol{r}}(x,t)\\&=\left\{\dot{u}_1+\dot{u}(x,t)\cos\theta_1-[a+x+u(x,t)]\sin\theta_1\dot{\theta}_1-\dot{v}(x,t)\sin\theta_1-v(x,t)\cos\theta_1\dot{\theta}_1\right\}\boldsymbol{i}\\&\quad+\left\{\dot{v}_1+\dot{u}(x,t)\sin\theta_1+[a+x+u(x,t)]\cos\theta_1\dot{\theta}_1+\dot{v}(x,t)\cos\theta_1-v(x,t)\sin\theta_1\dot{\theta}_1\right\}\boldsymbol{j}.\end{aligned} \tag{4}$$

The corresponding acceleration vector is given by

$$\begin{aligned}\boldsymbol{a}(x,t)&=\ddot{\boldsymbol{r}}(x,t)\\&=\Big\{\ddot{u}_1+\ddot{u}(x,t)\cos\theta_1-2\dot{u}(x,t)\sin\theta_1\dot{\theta}_1-2\dot{v}(x,t)\cos\theta_1\dot{\theta}_1-[a+x+u(x,t)]\sin\theta_1\ddot{\theta}_1\end{aligned}$$

$$
\begin{aligned}
&-\ddot{v}(x,t)\sin\theta_1-[a+x+u(x,t)]\cos\theta_1\dot{\theta}_1^2+v(x,t)\sin\theta_1\dot{\theta}_1^2-v(x,t)\cos\theta_1\ddot{\theta}_1\Big\}\boldsymbol{i}\\
&+\Big\{\ddot{v}_1+\ddot{u}(x,t)\sin\theta_1+2\dot{u}(x,t)\cos\theta_1\dot{\theta}_1-2\dot{v}(x,t)\sin\theta_1\dot{\theta}_1+[a+x+u(x,t)]\cos\theta_1\ddot{\theta}_1\\
&-[a+x+u(x,t)]\sin\theta_1\dot{\theta}_1^2+\ddot{v}(x,t)\cos\theta_1-v(x,t)\cos\theta_1\dot{\theta}_1^2-v(x,t)\sin\theta_1\ddot{\theta}_1\Big\}\boldsymbol{j}. \qquad (5)
\end{aligned}
$$

The contribution of a flexible beam to generalized active force is determined by the strain energy of the flexible beam during the docking process. The generalized active force is the partial derivative of strain energy to each independent speed variable.

Strain energy of the flexible beam is given by

$$
U=\frac{1}{2}E_1A\int_0^l\left(\frac{\partial u}{\partial x}\right)^2\mathrm{d}x+\frac{1}{2}E_1J\int_0^l\left(\frac{\partial^2 v}{\partial x^2}\right)^2\mathrm{d}x, \qquad (6)
$$

where E_1 is the Young's modulus of the beam, A is the cross-sectional area of the beam, and J is the sectional inertia moment of flexible beam.

The generalized active forces can be obtained by

$$
\begin{cases}
K_{fu_1}=-\dfrac{\partial U}{\partial u_1},\\
K_{fv_1}=-\dfrac{\partial U}{\partial v_1},\\
K_{f\theta_1}=-\dfrac{\partial U}{\partial \theta_1},\\
K_{fq_i}=-\dfrac{\partial U}{\partial q_i},\quad (i=1,2\ldots n).
\end{cases} \qquad (7)
$$

The detailed expressions of Eq. (7) can be obtained as follows:

$$
K_{fu_1}=0, \qquad (8)
$$

$$
K_{fv_1}=0, \qquad (9)
$$

$$
K_{f\theta_1}=0, \qquad (10)
$$

$$
\begin{aligned}
K_{fq_i}=&-\frac{1}{2}E_1A\int_0^l\left(\sum_{j=1}^n\varphi_j'(x)q_j(t)\right)^3\varphi_i'(x)\mathrm{d}x\\
&-E_1J\int_0^l\left(\sum_{j=1}^n\varphi_j''(x)q_j(t)\right)\varphi_i''(x)\mathrm{d}x,\ (i=1,2\ldots n). \qquad (11)
\end{aligned}
$$

According to the Kane method, the contribution of a flexible beam to the generalized inertia force is determined by

$$
\begin{cases}
K_{fu_1}^*=-\displaystyle\int_0^l\rho A\left(\frac{\partial \boldsymbol{V}(x,t)}{\partial \dot{u}_1}\right)\boldsymbol{a}(x,t)\mathrm{d}x,\\
K_{fv_1}^*=-\displaystyle\int_0^l\rho A\left(\frac{\partial \boldsymbol{V}(x,t)}{\partial \dot{v}_1}\right)\boldsymbol{a}(x,t)\mathrm{d}x,\\
K_{f\theta_1}^*=-\displaystyle\int_0^l\rho A\left(\frac{\partial \boldsymbol{V}(x,t)}{\partial \dot{\theta}_1}\right)\boldsymbol{a}(x,t)\mathrm{d}x,\\
K_{fq_i}^*=-\displaystyle\int_0^l\rho A\left(\frac{\partial \boldsymbol{V}(x,t)}{\partial \dot{q}_i}\right)\boldsymbol{a}(x,t)\mathrm{d}x,\quad (i=1,2\ldots n).
\end{cases} \qquad (12)
$$

The detailed expressions of Eq. (12) are written as follows:

$$K^*_{fu_1} = -\rho A \int_0^l \{\ddot{u}_1 - \{[a+x+u(x,t)]\sin\theta_1 + v(x,t)\cos\theta_1\}\ddot{\theta}_1 - 2\left[\dot{u}(x,t)\sin\theta_1 + \dot{v}(x,t)\cos\theta_1\right]\dot{\theta}_1 - \{[a+x+u(x,t)]\cos\theta_1 - v(x,t)\sin\theta_1\}\dot{\theta}_1^2 + \ddot{u}(x,t)\cos\theta_1 - \ddot{v}(x,t)\sin\theta_1\}\mathrm{d}x, \tag{13}$$

$$K^*_{fv_1} = -\rho A \int_0^l \{\ddot{v}_1 + \{[a+x+u(x,t)]\cos\theta_1 - v(x,t)\sin\theta_1\}\ddot{\theta}_1 + 2\left\{\dot{u}(x,t)\cos\theta_1 - \dot{v}(x,t)\sin\theta_1\right\}\dot{\theta}_1 - \{[a+x+u(x,t)]\sin\theta_1 + v(x,t)\cos\theta_1\}\dot{\theta}_1^2 + \ddot{u}(x,t)\sin\theta_1 + \ddot{v}(x,t)\cos\theta_1\}\mathrm{d}x, \tag{14}$$

$$\begin{aligned} K^*_{f\theta_1} = -\rho A \int_0^l \{\{-[a+x+u(x,t)]\sin\theta_1 - v(x,t)\cos\theta_1\}\ddot{u}_1 + \{[a+x+u(x,t)]\cos\theta_1 \\ - v(x,t)\sin\theta_1\}\ddot{v}_1 + \{[a+x+u(x,t)]^2 + v^2(x,t)\}\ddot{\theta}_1 + 2\{\dot{u}(x,t)\left[a+x+u(x,t)\right] \\ + \dot{v}(x,t)v(x,t)\}\dot{\theta}_1 - \ddot{u}(x,t)v(x,t) + \ddot{v}(x,t)\left[a+x+u(x,t)\right]\}\mathrm{d}x, \end{aligned} \tag{15}$$

$$\begin{aligned} K^*_{fq_i} = -\rho A \int_0^l \Bigg\{ \Bigg\{ -\int_0^x \left[\sum_{j=1}^n \varphi_j'(\sigma)q_j(t)\right]\varphi_i'(\sigma)\mathrm{d}\sigma\cos\theta_1 - \varphi_i(x)\sin\theta_1 \Bigg\}\ddot{u}_1 \\ + \Bigg\{ -\int_0^x \left[\sum_{j=1}^n \varphi_j'(\sigma)q_j(t)\right]\varphi_i'(\sigma)\mathrm{d}\sigma\sin\theta_1 + \varphi_i(x)\cos\theta_1 \Bigg\}\ddot{v}_1 \\ + \Bigg\{ [a+x+u(x,t)]\,\varphi_i(x) + v(x,t)\int_0^x \left[\sum_{j=1}^n \varphi_j'(\sigma)q_j(t)\right]\varphi_i'(\sigma)\mathrm{d}\sigma \Bigg\}\ddot{\theta}_1 \\ + 2\Bigg\{ \dot{u}(x,t)\varphi_i(x) + \dot{v}(x,t)\int_0^x \left[\sum_{j=1}^n \varphi_j'(\sigma)q_j(t)\right]\varphi_i'(\sigma)\mathrm{d}\sigma \Bigg\}\dot{\theta}_1 \\ + \Bigg\{ [a+x+u(x,t)]\int_0^x \left[\sum_{j=1}^n \varphi_j'(\sigma)q_j(t)\right]\varphi_i'(\sigma)\mathrm{d}\sigma - v(x,t)\varphi_i(x) \Bigg\}\dot{\theta}_1^2 \\ -\ddot{u}(x,t)\int_0^x \left[\sum_{j=1}^n \varphi_j'(\sigma)q_j(t)\right]\varphi_i'(\sigma)\mathrm{d}\sigma + \ddot{v}(x,t)\varphi_i(x) \Bigg\}\mathrm{d}x. \end{aligned} \tag{16}$$

The contributions of the satellite body are discussed then. In Figure 1(a), the displacement vector of o_1 is given by

$$\boldsymbol{r}_1 = u_1\boldsymbol{i} + v_1\boldsymbol{j}, \tag{17}$$

where μ_1 and v_1 are the coordinates in the inertia frame.

The corresponding velocity vector is given by

$$\dot{\boldsymbol{r}}_1 = \dot{u}_1\boldsymbol{i} + \dot{\boldsymbol{v}}_1\boldsymbol{j}. \tag{18}$$

The corresponding acceleration vector is given by

$$\boldsymbol{a}_{o_1} = \ddot{u}_1\boldsymbol{i} + \ddot{\boldsymbol{v}}_1\boldsymbol{j}. \tag{19}$$

The angular velocity vector is given by

$$\dot{\boldsymbol{\omega}}_1 = \dot{\theta}_1\boldsymbol{k}. \tag{20}$$

The partial velocities relative to $\dot{u}_1$, $\dot{v}_1$, and $\dot{\theta}_1$ are defined as

$$\boldsymbol{U}'_{o_1u_1} = \boldsymbol{i}, \quad \boldsymbol{U}'_{o_1v_1} = \boldsymbol{j}, \quad \boldsymbol{W}'_{1\theta_1} = \boldsymbol{k}. \tag{21}$$

From (17), (18) and (20), it is known that the partial velocities of satellite body relative to $\dot{q}_1, \dot{q}_2, \ldots, \dot{q}_n$ are zero. The external active force and moment are zero under the condition of space microgravity,

$$\boldsymbol{F}_{o_1} = \boldsymbol{0}, \quad \boldsymbol{M}_{o_1} = \boldsymbol{0}. \tag{22}$$

Therefore, the contributions of satellite body to the generalized active force are all zero,

$$K_{o_1u_1} = K_{o_1v_1} = K_{o_1\theta_1} = K_{o_1q_i} = 0, \ (i = 1, 2 \ldots n). \tag{23}$$

The inertia force vector can be obtained by

$$\boldsymbol{R}^*_{o_1} = -m_1\boldsymbol{a}_{o_1}. \tag{24}$$

The inertia moment vector can be obtained by

$$\boldsymbol{L}^*_{o_1} = -I_1\ddot{\theta}_1\boldsymbol{k}. \tag{25}$$

The contributions of satellite body to the generalized inertia force are obtained as follows:

$$\begin{cases} K^*_{o_1u_1} = \boldsymbol{R}^*_{o_1}\boldsymbol{U}'_{o_1u_1} = -m_1\ddot{u}_1, \\ K^*_{o_1v_1} = \boldsymbol{R}^*_{o_1}\boldsymbol{U}'_{o_1v_1} = -m_1\ddot{v}_1, \\ K^*_{o_1\theta_1} = L^*_{o_1}\boldsymbol{W}'_{1\theta_1} = -I_1\ddot{\theta}_1, \\ K^*_{o_1q_i} = 0, \quad (i = 1, 2, \ldots, n). \end{cases} \tag{26}$$

Finally, the Kane equations of the chaser satellite are obtained and shown as follows:

$$\begin{cases} K_{o_1u_1} + K_{fu_1} + K^*_{o_1u_1} + K^*_{fu_1} = 0, \\ K_{o_1v_1} + K_{fv_1} + K^*_{o_1v_1} + K^*_{fv_1} = 0, \\ K_{o_1\theta_1} + K_{f\theta_1} + K^*_{o_1\theta_1} + K^*_{f\theta_1} = 0, \\ K_{o_1q_i} + K_{fq_i} + K^*_{o_1q_i} + K^*_{fq_i} = 0, \quad (i = 1, 2, \ldots, n). \end{cases} \tag{27}$$

2.1.2 *Equations of the target satellite*

In Figure 1(a), the displacement vector of mass center of target satellite in the inertial frame can be written as

$$\boldsymbol{r}_2 = u_2\boldsymbol{i} + v_2\boldsymbol{j}, \tag{28}$$

where μ_2 and v_2 are the coordinate in the inertia frame.

The corresponding velocity vector is given by

$$\dot{\boldsymbol{r}}_2 = \dot{u}_2\boldsymbol{i} + \dot{v}_2\boldsymbol{j}. \tag{29}$$

The corresponding acceleration vector is given by

$$\boldsymbol{a}_{o_2} = \ddot{u}_2\boldsymbol{i} + \ddot{v}_2\boldsymbol{j}. \tag{30}$$

The angular velocity vector is given by

$$\dot{\boldsymbol{\omega}}_2 = \dot{\theta}_2\boldsymbol{k}. \tag{31}$$

Thus, three variables $(\dot{u}_2, \dot{v}_2, \dot{\theta}_2)$ are chosen to be the independent speed variables of the target satellite. The partial velocities relative to $\dot{u}_2$, $\dot{v}_2$, and $\dot{\theta}_2$ are defined as

$$\boldsymbol{U}'_{o_2u_2} = \boldsymbol{i}, \quad \boldsymbol{U}'_{o_2v_2} = \boldsymbol{j}, \quad \boldsymbol{W}'_{2\theta_2} = \boldsymbol{k}. \tag{32}$$

According to the Kane principle, contact force should be moved from inner cone surface to mass center of the target satellite. An additional moment vector will be the by-product of force translation.

The principal force vector in Figure 1(c) can be given by

$$\boldsymbol{F}_{o_2} = \{F_N \sin(\theta_2+\beta) + F_\tau \cos(\theta_2+\beta)\}\,\boldsymbol{i} + \{-F_N \cos(\theta_2+\beta) + F_\tau \sin(\theta_2+\beta)\}\,\boldsymbol{j}. \tag{33}$$

The additional moment vector can be given by

$$\boldsymbol{M}_{o_2} = \{F_N\,(b + R_2 \sin\beta + c\cos\beta) - F_\tau\,(c\sin\beta - R_2\cos\beta)\}\,\boldsymbol{k}. \tag{34}$$

Therefore, the generalized active forces relative to three independent speed variables $\dot{u}_2$, $\dot{v}_2$, and $\dot{\theta}_2$ can be obtained,

$$K_{o_2u_2} = \boldsymbol{F}_{o_2}\boldsymbol{U}'_{o_2u_2}, \quad K_{o_2v_2} = \boldsymbol{F}_{o_2}\boldsymbol{U}'_{o_2v_2}, \quad K_{o_2\theta_2} = \boldsymbol{M}_{o_2}\boldsymbol{W}'_{2\theta_2}. \tag{35}$$

In order to solve the generalized inertia forces, the inertia force vector and the inertia moment vector must be obtained firstly. The inertia force vector is obtained by

$$\boldsymbol{R}^*_{o_2} = -m_2\boldsymbol{a}_{o_2}. \tag{36}$$

The inertia moment vector is obtained by

$$\boldsymbol{L}^*_{o_2} = -I_2\ddot{\theta}_2\boldsymbol{k}. \tag{37}$$

Therefore, the generalized inertia forces relative to three independent speed variables $\dot{u}_2$, $\dot{v}_2$, and $\dot{\theta}_2$ are obtained by

$$K^*_{o_2u_2} = \boldsymbol{R}^*_{o_2}\boldsymbol{U}'_{o_2u_2}, \quad K^*_{o_2v_2} = \boldsymbol{R}^*_{o_2}\boldsymbol{U}'_{o_2v_2}, \quad K^*_{o_2\theta_2} = \boldsymbol{L}^*_{o_2}\boldsymbol{W}'_{2\theta_2}. \tag{38}$$

The Kane equations of the target satellite are obtained by

$$\begin{cases} K_{o_2u_2} + K^*_{o_2u_2} = m_2\ddot{u}_2 - F_N\sin(\theta_2+\beta) - F_\tau\cos(\theta_2+\beta) = 0, \\ K_{o_2v_2} + K^*_{o_2v_2} = m_2\ddot{v}_2 + F_N\cos(\theta_2+\beta) - F_\tau\sin(\theta_2+\beta) = 0, \\ K_{o_2\theta_2} + K^*_{o_2\theta_2} = I_2\ddot{\theta}_2 - F_N\,(b + R_2\sin\beta + c\cos\beta) + F_\tau\,(c\sin\beta - R_2\cos\beta) = 0. \end{cases} \tag{39}$$

Finally, the soft docking model of micro/small satellites using the Kane method is developed by combing (27) and (39). However, these above formulations are suitable only for the special docking situation when the motion of the central axes of the satellites stays in one plane.

2.1.3 *Formulation of contact force*

The distance from the top of the docking probe and the inner docking cone δ_N (along the normal direction of the inner cone surface) is used to determine the contact condition. The impact contact between probe and cone occurs on the condition $\delta_N \leqslant 0$. The impact force F_N is given by

$$F_N = F_k + F_d, \tag{40}$$

where F_k is the spring restoring force and F_d is the damping force.

The spring restoring force F_k is determined by Hertz contact theory,

$$F_k = \frac{4E^*\sqrt{R_e}}{3F_2^{\frac{3}{2}}(e)}\delta_N^{\frac{3}{2}}, \tag{41}$$

where

$$F_2(e) = \frac{2}{\pi}\left(\frac{b_c}{a_c}\right)^{\frac{1}{2}}\{F_1(e)\}^{-\frac{1}{3}}K(e), \tag{42}$$

$$F_1(e) = \frac{4}{\pi e^2}\left(\frac{b_c}{a_c}\right)^{\frac{3}{2}}\left\{\left[\left(\frac{a_c}{b_c}\right)^2 E(e) - K(e)\right][K(e) - E(e)]\right\}^{\frac{1}{2}}, \tag{43}$$

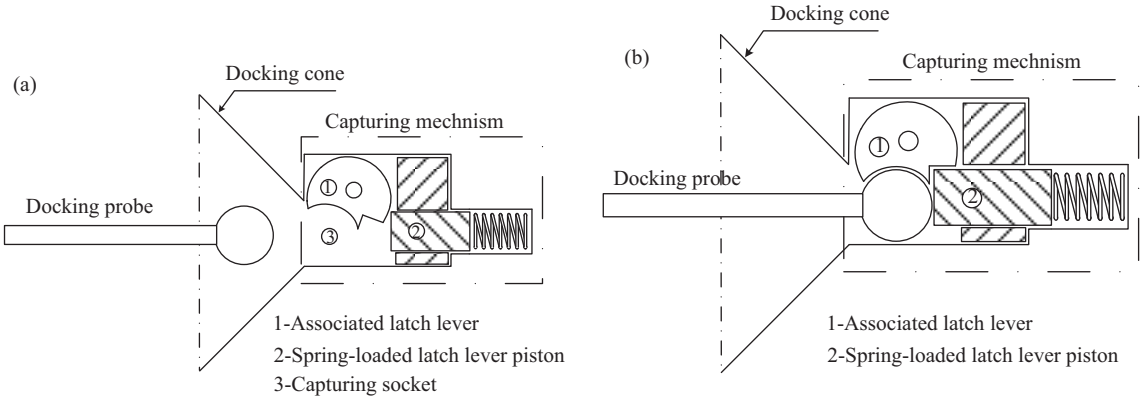

Figure 2 Operational principle of the capturing mechanism used in micro/small satellites. (a) Prior to capture and (b) captured.

$$\frac{b_c}{a_c} = \left(\frac{R''}{R'}\right)^{\frac{1}{2}}, \tag{44}$$

$$\frac{1}{E^*} = \frac{1-\mu_1^2}{E_1} + \frac{1-\mu_2^2}{E_2}, \tag{45}$$

$$R_e = (R'R'')^{\frac{1}{2}}, \tag{46}$$

where a_c is the semi-major axis of the contact ellipse and b_c is the minor semi-axis. e is the elliptic eccentricity, which is only related to the shape parameters of the ellipse. $K(e)$ and $E(e)$ are the first kind and the second kind of complete elliptic integral. R' and R'' are both relative main curvature radii. $R' = R'_1 \cdot R'_2/(R'_1 + R'_2)$, $R'' = R''_1 \cdot R''_2/(R''_1 + R''_2)$. μ_1 and μ_2 are Poisson ratios. E_1 and E_2 are Young's moduli. The geometric parameters of ball head and inner cone are separately $R'_1 = R''_1 = R_1$, $R'_2 = \infty$, and $R''_2 = R_2/\cos\beta$, where β is the cone angle.

The damping force F_d is determined as follows:

$$F_d = C_1 \delta_N \dot{\delta}_N, \tag{47}$$

where C_1 is the coefficient of damping.

The friction force in the tangential direction is obtained by the Columbus model, which is shown as follows:

$$F_\tau = \mu F_N, \tag{48}$$

where μ is the frictional coefficient.

2.2 Evaluation of a successful docking

The above analytical model allows us to study the effect of the contact parameters that govern the soft docking of micro (or small) paired satellites. Since the final aim of soft docking is to connect the two satellites using a capturing mechanism, it is appropriate to summarize the operational principle of the capturing mechanism used in the docking of micro (or small) paired satellites.

Figure 2 shows the two phases of the capture operation of micro (or small) paired satellites: prior to capture (Figure 2(a)) and captured (Figure 2(b)). Figure 2 shows that the capturing mechanism can be activated only when the spherical end of the docking probe closely approaches the capturing socket (③ in Figure 2(a)) with an appropriate positive relative velocity. This allows a spring loaded latch lever to capture the docking arm. Accordingly, the following conditions are defined to predict whether a successful or unsuccessful docking event will take place using the current VI approach:

(i) The trajectory of the docking probe is within the docking cone.

(ii) The spherical-end of the docking probe contacts the docking cone and slides into the capture zone.

(iii) The relative velocity between the chaser satellite and the target satellite allows engagement.

Table 1 Parameters of soft docking model

Item	Symbol and value			
Chaser satellite	E_1=210 GPa	v_1=0.33	ρ_1=7850 kg/m^3	l_1=0.2 m
	E_p=70 GPa	$v_p = 0.33$	ρ_p=2740 kg/m^3	d_p=0.012 m
	l_p=0.2 m	R_p=0.01 m		
Target satellite	m_2=67.630 kg	I_2=2.4671 kg $\cdot$ m^2	l_2=0.2 m	c=0.16 m
	$\beta = \pi 8/4$	b=0.045 m	R_2=0.015 m	l_3=0.0707 m

(iv) The compliance of the docking probe is such that it will facilitate successful docking.

In order to implement the above conditions, two relative velocities need to be defined. The first is the relative docking velocity ($V_{\rm rd}$) of the paired satellites during the entire docking process. It is the relative velocity of the mass center of the chaser satellite along the central axis direction of the target satellite and can be expressed as follows:

$$V_{\rm rd} = (V_{1x} - V_{2x})\cos(\theta_2) + (V_{1y} - V_{2y})\sin(\theta_2), \tag{49}$$

where V_{1x} and V_{1y} denote the center-of-mass velocities of the chaser satellite along X and Y axes in the inertial reference frame (refer to Figure 1). The velocities V_{2x} and V_{2y} denote the center-of-mass velocities of the target satellite along X and Y axes in the inertial reference frame (refer to Figure 1). θ_2 is the rotational angle of the target satellite.

The second is the final relative docking velocity of the paired-satellites just prior to capture. This velocity will be called the relative capturing velocity ($V_{\rm rc}$). According to the conditions needed to guarantee successful docking, the relative capturing velocity must satisfy the following inequality:

$$V_{\rm rc\,min} \leqslant V_{\rm rc} \leqslant V_{\rm rc\,max}. \tag{50}$$

When the relative capturing velocity is lower than a certain value ($V_{\rm rc} < V_{\rm rc\,min}$), the capture mechanism may not be activated. The upper limit $V_{\rm rc\,max}$ is restricted by the buffering capacity of the spring-based capturing mechanism.

2.3 Comparison of predictions with a commercial code

To obtain the relative docking velocity ($V_{\rm rd}$) and the relative capturing velocity ($V_{\rm rc}$), it is necessary to calculate the velocity components of the paired satellites along the respective X and Y directions (V_{1x}, V_{1y}, V_{2x}, and V_{2y}) as well as the rotational angle of the target satellite (θ_2) according to Eq. (49). In the following, the predictions of these results (V_{1x}, V_{1y}, V_{2x}, V_{2y}, and θ_2) given by the newly developed model and the commercial FE package (ANSYS LSDYNA) were conducted and compared. The simulations were carried out using the parameters of the micro (or small) paired satellites system listed in Table 1.

The definitions of the above symbols can be found in the Nomenclature. In the current example, the friction coefficient of the candidate contact surfaces between the docking probe and the docking cone was taken as $\mu = 0.3$. Considering that the soft docking design is helpful in lowering the requirement to the satellite attitude control system, the initial relative docking speed of the two satellites is assumed to be a little higher than the typical value. Thus, the initial velocity of the chaser satellite was assumed to be $V_{1x} = 0.4$ m/s, along the X direction (refer to Figure 1). The target satellite was assumed to be initially static. An incremental time step of $\Delta t = 1 \times 10^{-4}$ s was adopted to balance the calculation efficiency and precision.

Figure 3 shows the predicted results obtained from the new model and ANSYS LSDYNA. The contact solution used in LSDYNA is a penalty-based contact algorithm. The accuracy of the contact solution given by LSDYNA depends on the user-defined contact stiffness factor. In order to validate the results obtained from LSDYNA, three types of stiffness factor (SF = 1, SF = 1×10^{-2}, and SF = 1×10^{-5}) are chosen. It can be seen that the results in cases of SF = 1 and SF = 1×10^{-2} show good agreement. Thus, the predicted results from LSDYNA (SF = 1) are chosen to validate the correctness of the newly proposed model. In Figure 3(a) and (b), the mass center velocities of the paired satellites along X and

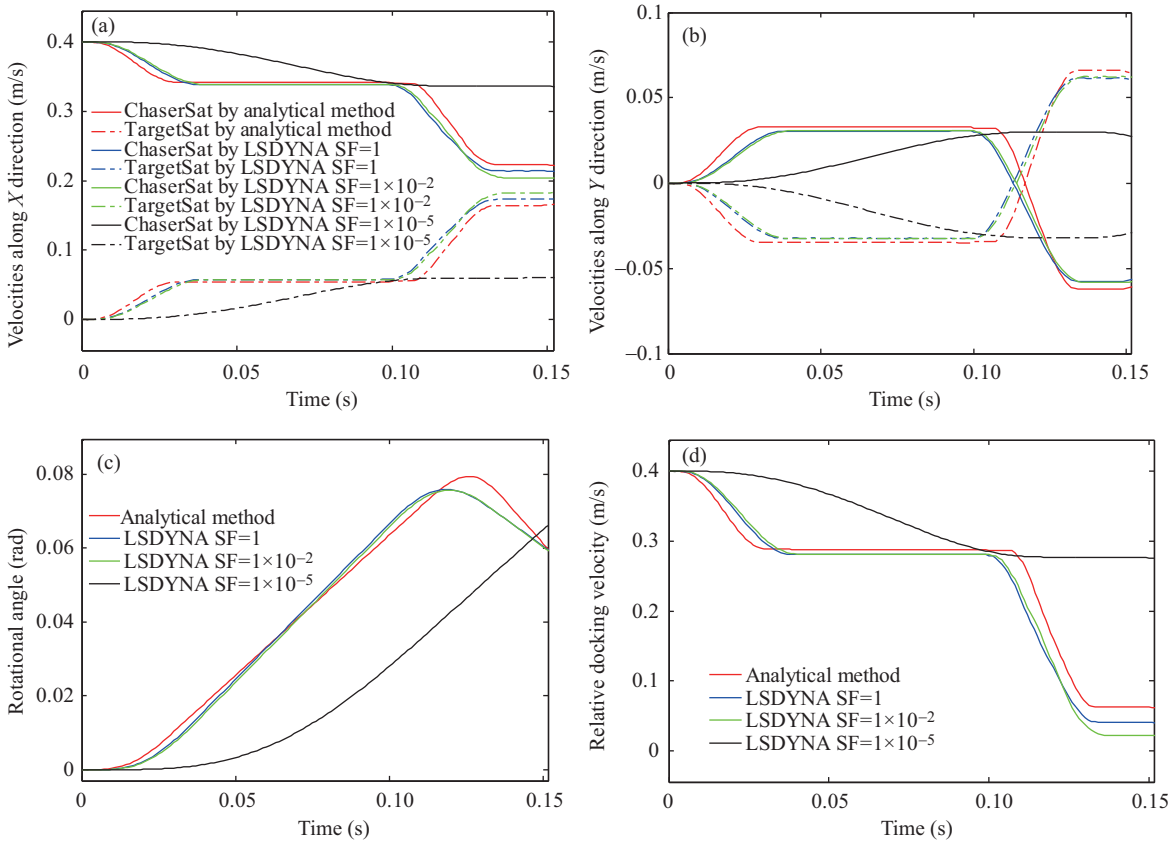

Figure 3 (Color online) Comparison of the predicted results between the newly developed model and the commercial code LSDYNA. The velocity components along the respective X (a) and Y (b) directions of the paired satellites (V_{1x}, V_{1y}, V_{2x}, V_{2y}), (c) rotational angle θ_2 of the target satellite, and (d) relative docking velocity $V_{\rm rd}$.

Y axes, including V_{1x}, V_{1y}, V_{2x}, and V_{2y} (refer to Figure 1) versus time are given. It can be seen that the variations in V_{1x}, V_{1y}, V_{2x}, and V_{2y} occur during every impact-contact. After every impact-contact, there is no external force loaded on the satellites, and the mass center velocities of the chaser satellite and the target satellite along X and Y directions (V_{1x}, V_{1y}, V_{2x}, and V_{2y}) remain constant. In Figure 3(c), the rotational angle θ_2 of the target satellite versus time is given. Once the velocities (V_{1x}, V_{1y}, V_{2x}, and V_{2y}) and the angle (θ_2) are obtained, the relative docking velocity ($V_{\rm rd}$) can be calculated according to (49), which is shown in Figure 3(d). From Figure 3, it is observed that the predictions of the newly proposed model agree well with ANSYS LSDYNA. It proves the accuracy of the new model in predicting the velocities of the paired satellites.

3 Parameters analysis and design

3.1 Effect of three factors of the docking system

This investigation involves the choice of three parameters to be the main factors that govern soft docking, including the bending stiffness (EI) of the docking probe, the angle (β) of the docking cone, and the friction coefficient (μ) of the candidate contact surfaces. Firstly, the independent effects of the above three factors are examined using the elastic and geometry parameters given in Table 1. The simulation results are depicted in Figures 4–6.

Figure 4 shows the effect of probe bending stiffness (EI) on the relative docking velocity ($V_{\rm rd}$) and relative capturing velocity ($V_{\rm rc}$) of the paired satellites. In Figure 4(a), five cases of EI are chosen, and their effects on $V_{\rm rd}$ are given. Observing the value of $V_{\rm rd}$ just prior to capture, $V_{\rm rc}$ is obtained in the five cases of EI (shown in Figure 4(b)). It is noted that $V_{\rm rc}$ decreases with the increase of EI.

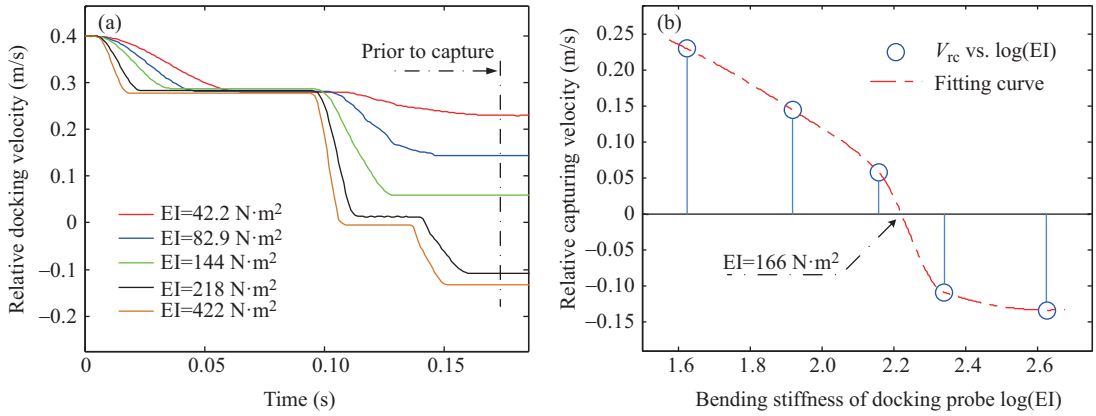

Figure 4 (Color online) Effect of the probe bending stiffness (EI) on velocities of the paired satellites. (a) Relative docking velocity (V_{rd}), and (b) relative capturing velocity (V_{rc}).

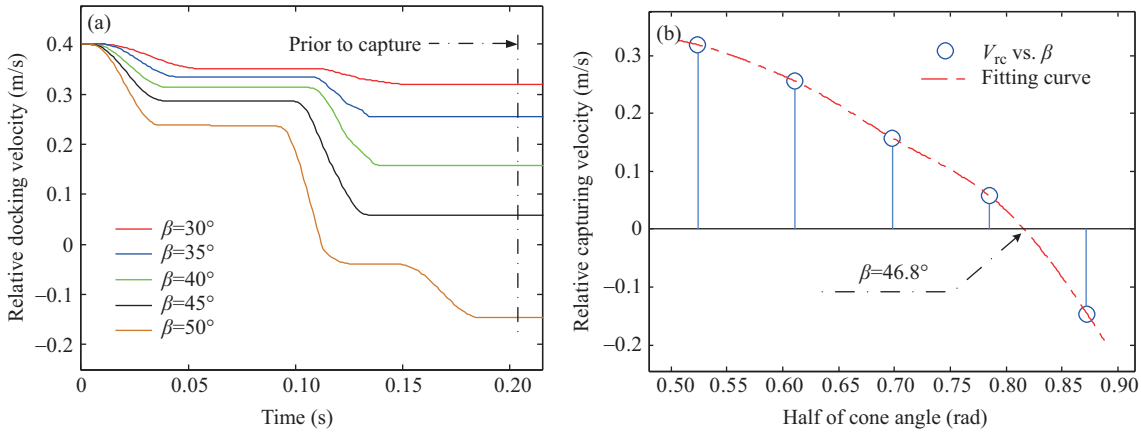

Figure 5 (Color online) Effect of the cone angle (β) on velocities of the paired satellites. (a) Relative docking velocity (V_{rd}), and (b) relative capturing velocity (V_{rc}).

Moreover, V_{rc} becomes negative in cases with a comparatively large EI (218 N $\cdot$ m^2, 422 N $\cdot$ m^2). Using the shape-preserving interpolant, the fitting curve of V_{rc} versus the logarithm of EI is obtained, shown in Figure 4(b). Then the switching point that divides the positive and the negative value of V_{rc} can be obtained. The value of EI on this point is 166 N $\cdot$ m^2. When the bending stiffness EI is smaller than this switching value, the spherical end of the docking probe will reach the capture socket of the docking cone with a positive V_{rc}. In case of an EI larger than the switching point, V_{rc} becomes negative, which means that the chaser satellite will bounce away from the target satellite with an unsuccessful docking operation.

Figure 5 shows the effect of cone angle (β) on the relative docking velocity (V_{rd}) and relative capturing velocity (V_{rc}) of the paired satellites. It is noted that V_{rc} decreases with the increase of β. From the fitting curve shown in Figure 5(b), the value of β on the switching point is 46.8°. The spherical end of the docking probe can reach the capture socket when β is smaller than this switching value.

Figure 6 shows the effect of friction coefficient (μ) on the relative docking velocity (V_{rd}) and relative capturing velocity (V_{rc}) of the paired satellites. It is noted that V_{rc} decreases with the increase of μ. The switching value of μ obtained from the fitting curve in Figure 6(b) is 0.345, which can be used to design the surface conditions of the spherical end of the docking probe and the inner docking cone.

3.2 Parameter design

According to the above analysis, it is known that all these three factors (EI, β, and μ) have significant effects on the relative capturing velocity (V_{rc}) of the paired satellites. Based on model simulations, V_{rc}

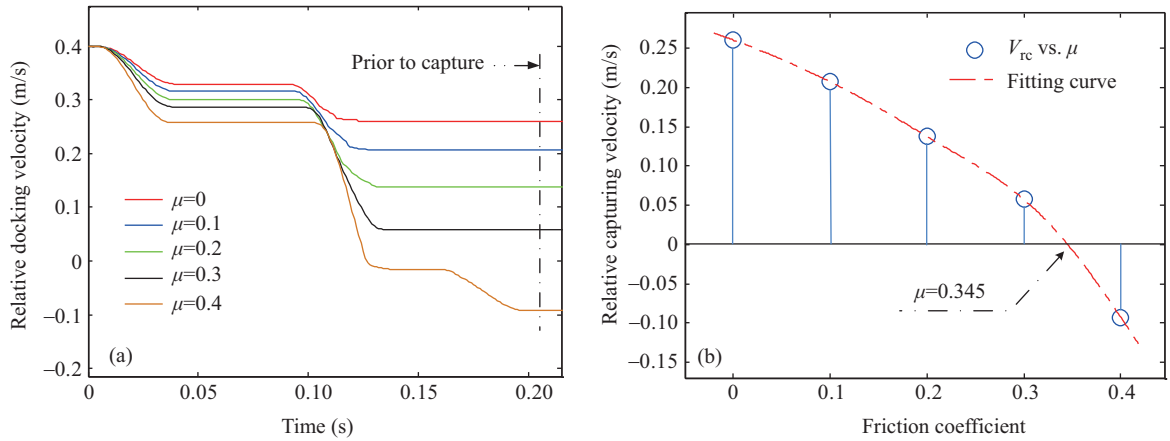

Figure 6 (Color online) Effect of the friction coefficient (μ) on velocities of the paired satellites. (a) Relative docking velocity ($V_{\rm rd}$), and (b) relative capturing velocity ($V_{\rm rc}$).

Table 2 Variation of three factors

Case	1	2	3	4	5	6	7	8	9
EI (N·m^2)	4.22	8.29	14.4	21.8	42.2	82.9	144	218	422
β(°)	30	32.5	35	37.5	40	42.5	45	47.5	50
μ	0	0.05	0.1	0.15	0.2	0.25	0.3	0.35	0.4

Table 3 $V_{\rm rc}$ versus EI and β (m/s)

		EI (N·m^2)								
		4.22	8.29	14.4	21.8	42.2	82.9	144	218	422
β (°)	30	0.383	0.3842	0.3869	0.3797	0.3792	0.3779	0.379	0.3781	0.3765
	32.5	0.3637	0.3613	0.367	0.3558	0.3536	0.35	0.3459	0.3438	0.3398
	35.0	0.3541	0.3479	0.3477	0.3342	0.3266	0.3224	0.3114	0.3067	0.2995
	37.5	0.3539	0.3449	0.3227	0.323	0.3132	0.3	0.2845	0.2729	0.257
	40.0	0.324	0.3139	0.3006	0.2885	0.2749	0.2555	0.2299	0.2037	0.166
	42.5	0.2972	0.2831	0.2623	0.2499	0.2269	0.1976	0.145	0.102	0.049
	45.0	0.263	0.2415	0.2106	0.191	0.158	0.075	0.043	−0.053	−0.107
	47.5	0.229	0.1996	0.165	0.127	0.087	−0.091	−0.108	−0.125	−0.143
	50.0	0.2305	0.2013	0.166	0.127	−0.047	−0.09	−0.108	−0.122	−0.139

Table 4 $V_{\rm rc}$ versus EI and μ (m/s)

		EI (N·m^2)								
		4.22	8.29	14.4	21.8	42.2	82.9	144	218	422
μ	0	0.3725	0.3695	0.365	0.36	0.3557	0.35	0.3459	0.3389	0.3306
	0.05	0.3533	0.3475	0.3418	0.335	0.3282	0.32	0.3114	0.301	0.2903
	0.10	0.3359	0.329	0.3211	0.312	0.3054	0.2945	0.2845	0.272	0.2605
	0.15	0.3283	0.32	0.3147	0.3065	0.298	0.2878	0.2785	0.2678	0.2567
	0.20	0.3263	0.3167	0.3033	0.2875	0.2703	0.25	0.2299	0.2025	0.171
	0.25	0.3071	0.2901	0.2686	0.2439	0.2161	0.182	0.145	0.093	0.046
	0.30	0.2607	0.2354	0.2071	0.172	0.138	0.093	0.043	0.011	−0.015
	0.35	0.2088	0.172	0.141	0.053	−0.033	−0.067	−0.102	−0.113	−0.128
	0.40	0.16	0.08	−0.016	−0.033	−0.066	−0.087	−0.108	−0.114	−0.126

was obtained at the following values of EI, β, and μ, which are listed in Table 2.

The corresponding relative capturing velocities ($V_{\rm rc}$) are listed in Tables 3 and 4.

In order to compare the results clearly, the logarithm of EI and the radian of β are adopted to make the three factors appear in a similar order of magnitude. The surface fitting and the contour chart based

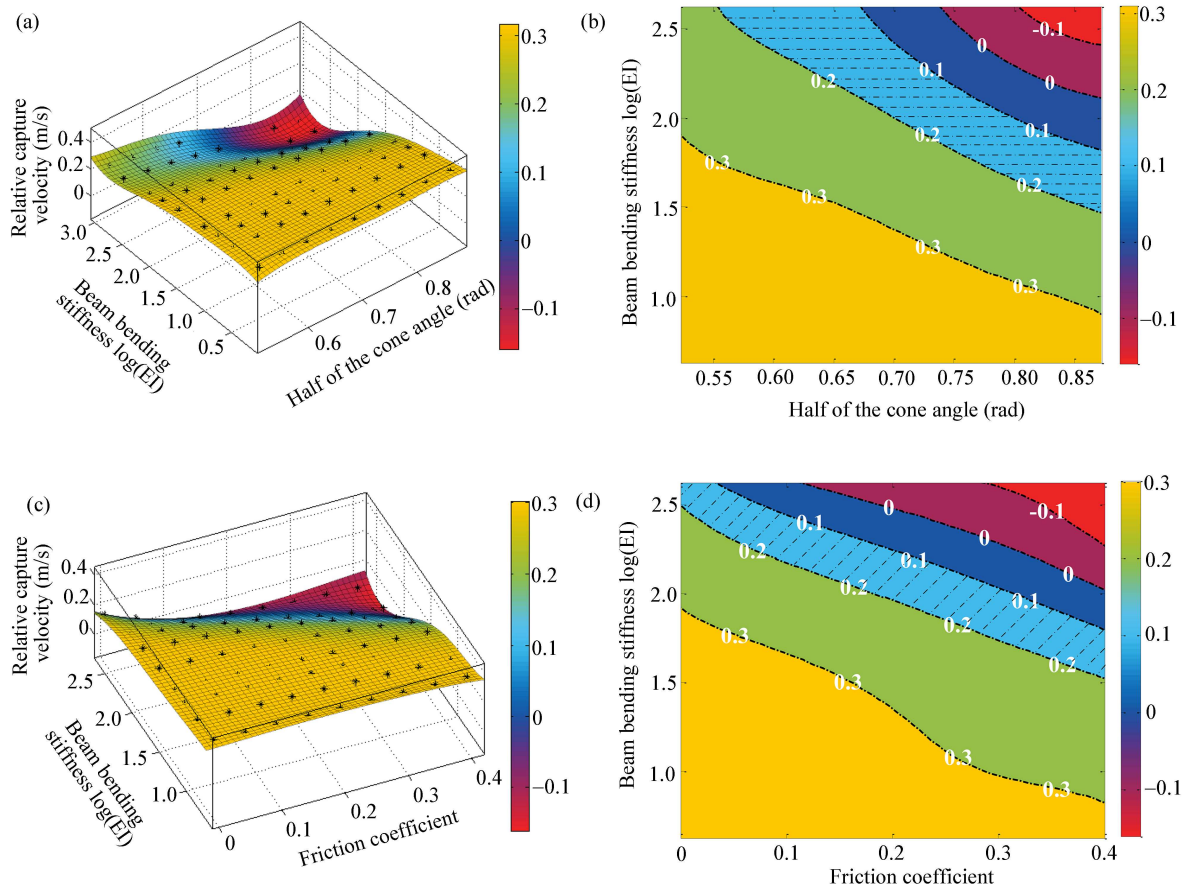

Figure 7 (Color online) Contact design domains. (a) Fitting chart and (b) contour chart in terms of probe bending stiffness (EI) and cone angle (β); (c) fitting chart and (d) contour chart in terms of probe bending stiffness (EI) and friction coefficient (μ).

on the obtained $V_{\rm rc}$ are shown in Figure 7.

Figure 7 shows that the value of $V_{\rm rc}$ changes with the variation in EI, β, and μ. The surface fitting chart of $V_{\rm rc}$ in terms of EI and β is shown in Figure 7(a). Its corresponding contour chart is shown in Figure 7(b). The surface fitting and contour charts of $V_{\rm rc}$ vs EI and μ are shown in Figure 7(c) and (d), respectively. It is observed that the contour charts in Figure 7(b) and (d) show obviously zonal distributions, and they can be used to design the domains of these three factors (EI, β, and μ) for a successful docking once we know the upper ($V_{\rm rc\,max}$) and lower ($V_{\rm rc\,min}$) limits of $V_{\rm rc}$ in (50). For example, if $V_{\rm rc\,min} = 0.1$ m/s and $V_{\rm rc\,max} = 0.2$ m/s, then the shaded zones of 0.1 m/s $\leqslant V_{\rm rc} \leqslant$ 0.2 m/s in Figure 7(b) and (d) are the required domains. By proper design, the values of EI, β, and μ can be adjusted in the domains for the successful docking of micro (or small) paired satellites.

4 Conclusion

This investigation focused on the main governing parameters that affect the capture results for a soft docking of micro (or small) paired satellites using our proposed model. In order to estimate the docking and capturing results, we defined the relative docking and capturing velocities by considering the operational principle of the capturing mechanism used in micro (or small) paired satellites. Next, the effects of the bending stiffness of the docking probe, the angle of the docking cone and the friction coefficient of the candidate contact surfaces on the relative docking and capturing velocities were examined. Using the relative capturing velocity as the design object, the available domains of these three factors were

determined. These design domains provide a guideline to improve the properties of the soft docking system developed for micro (or small) paired satellites.

Acknowledgements This work was supported by National Natural Science Foundation of China (Grant Nos. 91216201, 51205403, 11404405).

Conflict of interest The authors declare that they have no conflict of interest.

References

1 Wiens G J, Umsrithong A, Miller S, et al. Design of autonomous foldable docking mechanism for small space vehicles. In: Proceedings of the International Design Engineering Technical Conferences and Computers and Information in Engineering Conference, California, 2009. 1–10
2 Barbetta M, Boesso A, Branz F, et al. ARCADE-R2 experiment on board BEXUS 17 stratospheric balloon. CEAS Space J, 2015, 7: 1–12
3 Boesso A, Francesconi A. ARCADE small-scale docking mechanism for micro-satellites. Acta Astronautica, 2013, 86: 77–87
4 Barker W F. Magnetic docking probe for soft docking of space vehicles. US Patent, 4381092, 1983-04-26
5 Zhang X, Huang Y Y, Han W, et al. Research of flexible beam impact dynamics based on space probe-cone docking mechanism. Adv Space Res, 2012, 49: 1053–1061
6 Yoo H H, Seo S, Huh K. The effect of a concentrated mass on the modal characteristics of a rotating cantilever beam. Proc Inst Mech Eng Part C: J Mech Eng Sci, 2002, 216: 151–163
7 Yoo H H, Shin S H. Vibration analysis of rotating cantilever beams. J Sound Vib, 1998, 212: 807–828
8 Dong F-X, Hong J Z, Zhu K, et al. Numerical and experimental studies on impact dynamics of a planar flexible multibody system. Acta Mech Sin, 2010, 26: 635–642
9 Guo A P, Hong J Z, Yang H. A dynamic model with substructures for contact-impact analysis of flexible multibody systems. Sci China Ser E-Tech Sci, 2003, 46: 33–40
10 Kane T R, Ryan R R, Banerjeer A K. Dynamics of a cantilever beam attached to a moving base. J Guid, 1987, 10: 139–151
11 Pellicano F, Vestroni F. Nonlinear dynamics and bifurcations of an axially moving beam. J Vib Acoust, 2000, 122: 21–30
12 Lim H S, Kwon S H, Yoo H H. Impact analysis of a rotating beam due to particle mass collision. J Sound Vib, 2007, 308: 794–804
13 Zhang G H, Liu Z S, Yoo H H. In-plane vibration analysis of cantilevered circular arc beams undergoing rotational motion. J Mech Sci Tech, 2008, 22: 113–119
14 Teng Y-Y, Cai G-P. Frequency characteristics of a flexible hub-beam system with arbitrary settling position of attached mass. J Vib Control, 2007, 13: 769–794
15 Seo S, Yoo H H. Dynamic analysis of flexible beams undergoing overall motion employing linear strain measures. AIAA J, 2002, 40: 319–326
16 Cai G-P, Hong J-Z, Yang S X. Dynamic analysis of a flexible hub-beam system with tip mass. Mech Res Commun, 2005, 32: 173–190
17 Ni Q, Li M, Tang M, et al. Free vibration and stability of a cantilever beam attached to an axially moving base immersed in fluid. J Sound Vib, 2014, 333: 2543–2555
18 Xi L Y, Li X F, Tang G J. Free vibration of standing and hanging gravity-loaded Rayleigh cantilevers. Int J Mech Sci, 2013, 66: 233–238
19 Olivieri L, Francesconi A. Design and test of a semiandrogynous docking mechanism for small satellites. Acta Astron, 2016, 122: 219–230
20 Li J-G, Ding J, Yao Y-X, et al. A new accuracy design for a 6-dof docking mechanism. Proc Inst Mech Eng Part C: J Mech Eng Sci, 2015, 229: 3473–3483
21 Lai Y N, Dai Y, Tian H, et al. Design of an automatic autonomous mini prone-cone microsatellite docking mechanism. Chin J Mech Eng, 2010, 23: 353–360
22 Chen C Z, Nie H, Chen J B, et al. A velocity-based impedance control system for a low impact docking mechanism (LIDM). Sensors, 2014, 14: 22998–23016